Current-phase relations in SIsFS junctions in the vicinity of 0-π transition

S. V. Bakurskiy,[1,2,3] V. I. Filippov,[4,5] V. I. Ruzhickiy,[4] N. V. Klenov,[2,4,5] I. I. Soloviev,[1,2]
M. Yu. Kupriyanov,[1,2,3] and A. A. Golubov[2,6]

[1]*Skobeltsyn Institute of Nuclear Physics, Lomonosov Moscow State University 1(2), Leninskie gory, Moscow 119234, Russian Federation*
[2]*Moscow Institute of Physics and Technology, Dolgoprudny, Moscow Region, 141700, Russian Federation*
[3]*National University of Science and Technology MISIS, 4 Leninsky prosp., Moscow, 119049, Russia*
[4]*Faculty of Physics, M.V. Lomonosov Moscow State University, 119992 Leninskie Gory, Moscow, Russia*
[5]*All-Russian Research Institute of Automatics n.a. N.L. Dukhov (VNIIA), 127055, Moscow, Russia*
[6]*Faculty of Science and Technology and MESA+ Institute for Nanotechnology, University of Twente, 7500 AE Enschede, The Netherlands*

We consider the current-phase relation (CPR) in Josephson junctions with complex insulator-superconductor-ferromagnetic interlayers in the vicinity of the 0-π transition. We find a strong impact of the second harmonic on the CPR of the junctions. It is shown that the critical current can be kept constant in the region of 0-π transition, while the CPR transforms through multivalued hysteretic states depending on the relative values of tunnel transparency and magnetic thickness. Moreover, the CPR in the transition region has multiple branches with distinct ground states.

I. INTRODUCTION

The current-phase relation (CPR) $I_S(\varphi)$ between a supercurrent I_S and a phase difference φ is the most basic property of a Josephson junction [1,2]. It is well-known that the CPR in a superconductor-insulator-superconductor (SIS) type junction has a sinusoidal shape at arbitrary temperatures. In the superconductor-normal-superconductor (SNS), superconductor-ferromagnetic-superconductor (SFS) junctions, or double-barrier SINIS structures, deviations from this behavior occur at temperatures much smaller than the critical temperature T_C of S electrodes, T_C. At the same time, in all these structures, $I_S(\varphi)$ is a single-valued function of φ, irrespective of the transport properties and the geometry of the weak-link region [2].

Previously, it was shown that the situation might be different when the weak link is formed by a material which is intrinsically superconducting (s) with a transition temperature lower than that of the S electrodes. In this case, an increase of the distance between the electrodes may result in the transformation [3] of $I_S(\varphi)$ from single- to multi-valued function of φ. The parameter range for which this transformation takes place, defines the transition from the Josephson effect to the Abrikosov vortex flux flow in the film [4].

Recent theoretical [5] and experimental [6] studies indicated a possible realization of the above mentioned transformations of $I_S(\varphi)$ in SIsFS structures in the form of instabilities near a 0-π transition. So far, this new fundamental feature of the Josephson structures remains unexplored. In this paper we address this problem by considering the properties of an SIsFS junction in the vicinity of a 0-π transition taking into account the existence of a significant second harmonic of current-phase relation (CPR) in the sFS part of the structure.

We find that the 0-π transition in SIsFS structures is going through distinct states with a discontinuous hysteretic current-phase relation. Moreover, protected 0 and π states are found in the system with multiple possible branches of current phase relation. Finally, we demonstrate that the 0-π transition can be realized without changes of the critical current due to a

transformation of the current-phase relations, which hinders an observation of this transition in the conventional manner and requires phase sensitive experiments [7].

The paper is organized as follows. In Sec. II, two theoretical models, a microscopic and a phenomenological one, are formulated, which describe the CPR in SIsFS structures and the results of these two approaches are compared. Sections III and IV provide analytical and numerical results for CPR followed from the lumped contacts model. The classification of the physical states in the SIsFS structures is introduced in terms of a number of the ground states and shapes of $I_S(\varphi)$ curves.

II. THEORETICAL MODEL OF SISFS STRUCTURE

Below, we will use two complementary approaches for solving the problem. The first one is based on a microscopic theory of superconductivity and employs numerical simulation of the processes in the structure within the framework of the Usadel equations [8] with Kupriyanov-Lukichev boundary conditions [9] at the interfaces:

$$\frac{\pi T_C \xi_p^2}{\widetilde{\omega}_p G_m} \frac{d}{dx}\left(G_p^2 \frac{d\Phi_p}{dx} \right) - \Phi_p = -\Delta_p, \tag{1}$$

$$\Delta_p \ln \frac{T}{T_C} + \frac{T}{T_C} \sum_{\omega=-\infty}^{\infty} \left(\frac{\Delta_p}{|\omega|} - \frac{\Phi_p G_p}{\omega} \right) = 0, \tag{2}$$

$$\pm \gamma_{Bpq} \xi_p G_p \frac{d}{dx} \Phi_p = G_q \left(\frac{\widetilde{\omega}_p}{\widetilde{\omega}_q} \Phi_q - \Phi_p \right). \tag{3}$$

Here, p and q are subscripts of the corresponding layers, $G_p = \widetilde{\omega}_p / \sqrt{\widetilde{\omega}_p^2 + \Phi_{p,\omega}\Phi_{p,-\omega}^*}$, $\widetilde{\omega}_p = \omega + iH_p$, $\omega = \pi T(2n + 1)$ are the Matsubara frequencies, Δ_p is the pair potential that exists inside the superconductors, H_p is the exchange energy of the ferromagnetic layer ($H_p = 0$ in nonferromagnetic materials), T_C is the critical temperature of superconductors, $\xi_p = (D_p/2\pi T_C)^{1/2}$ is the coherence length, D_p is the diffusion coefficient, G_p and Φ_p are the normal and anomalous
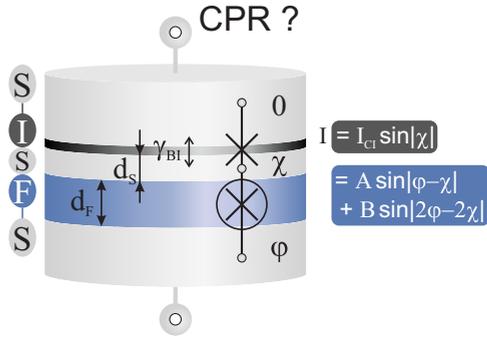
FIG. 1. Sketch of the SIsFS structure with an equivalent scheme for the lumped elements method.

Green's functions, respectively, $\gamma_{Bpq} = R_{Bpq} \mathcal{A}_{Bpq} / \rho_p \xi_p$ is the suppression parameter, R_{Bpq} and $\mathcal{A}_{Bpq}$ are the resistance and area of the corresponding interface. The sign plus in (3) means that pth material is located at the side $x_i - 0$ from interface position x_i, and sign minus corresponds to the case when the pth material is at $x_i + 0$. The x axis is oriented perpendicular to the interfaces. At the free surfaces of the S electrodes located far away from the boundaries ($x \rightarrow \pm \infty$), we set the bulk values of the Green function in the superconductor $\Phi = \Delta_0 \exp(i\psi)$ with $\psi = 0$ and $\psi = \varphi$.

The boundary problem (1)–(3) was solved numerically by making use of the algorithm developed in Ref. [5]. Calculated Green's functions were used to find a current across a SIsFS junction as a function of the phase difference φ:

$$\frac{2eI_S(\varphi)}{\pi T \mathcal{A}_B} = \sum_{\omega = -\infty}^{\infty} \frac{iG_{p,\omega}^2}{\rho_p \widetilde{\omega}_p^2} \left(\Phi_{p,\omega} \frac{\partial \Phi_{p,-\omega}^*}{\partial x} - \Phi_{p,-\omega}^* \frac{\partial \Phi_{p,\omega}}{\partial x} \right). \tag{4}$$

The second approach is a phenomenological one. It is based on modeling the structure as a system of two lumped contacts connected in series (see Fig. 1): the SIs junction with conventional sinusoidal CPR $I_{SIs} = I_{CI} \sin(\chi)$ and an sFS junction which has CPR

$$I_{sFS} = A \sin(\varphi - \chi) + B \sin(2(\varphi - \chi)) \tag{5}$$

having both the first and the second harmonics. Within this model, the amplitudes A and B are considered as independent parameters, while the phase difference on tunnel layer χ is a function of the phase drop on the whole junction φ. The $\chi(\varphi)$ dependence can be found from the condition of the current equality across SIs and sFS junctions:

$$I_{CI} \sin(\chi) = A \sin(\varphi - \chi) + B \sin(2(\varphi - \chi)). \tag{6}$$

The lumped contacts model is applicable [5] for $d_S > \pi^2 \xi_S / (4\sqrt{1 - T/T_C})$.

For arbitrary relations between I_{CI}, A, and B, Eq. (6) for $\chi(\varphi)$ has been solved numerically, thus determining the current-phase $I_S(\varphi) = I_{CI} \sin(\chi)$ and the energy-phase

relations

$$E(\varphi) = \frac{\Phi_0 I_{CI}}{2\pi} (1 - \cos(\chi)) + E_A + E_B,$$

$$E_A = \frac{\Phi_0 A}{2\pi} (1 - \cos(\varphi - \chi)),$$

$$E_B = \frac{\Phi_0 B}{4\pi} (1 - \cos(2(\varphi - \chi))). \tag{7}$$

Generally, Eq. (6) has several independent solutions for $\chi(\varphi)$ in the interval $0 \leqslant \varphi \leqslant 2\pi$. However, only some of these solutions meet the stability criterion

$$\frac{d^2 E(\chi)}{d\chi^2} = \cos(\chi) + \frac{A}{I_{CI}} \cos(\varphi - \chi)$$

$$+ \frac{2B}{I_{CI}} \cos(2(\varphi - \chi)) > 0, \tag{8}$$

which means that the solution is stable if the functional $E(\chi)$ for certain φ is at a local minimum.

In Fig. 2(a), we compare $I_S(\varphi)$ dependencies calculated in the frame of both approaches. The solution of Usadel equations has been found for the following set of parameters: $d_F = 0.46\xi_S$, $d_s = 5\xi_S$, $H = 10\pi T_C$, $T = 0.2T_C$, the suppression parameters at SIs and SF interfaces are equal to $\gamma_{BI} = 1000$ and $\gamma_{BSF} = 0.3$, respectively. The resulting $I_S(\varphi)$ dependence of SIsFS contact is shown in Fig. 2 by the open circles. It can be seen that there are two critical points in $I_S(\varphi)$ curve at which there is a stepwise change of the supercurrent. They are located at $\varphi/2\pi \approx 0.2$; 0.8.

In the spirit of the lumped junction model, one has to find the characteristics of SIs and sFS parts of the SIsFS structure independently from each other. For the SIs tunnel junction we get $I_{CI} = 0.88\pi T_C / R_N$. Microscopic calculations for the sFS structure demonstrate that it is in the vicinity of the 0-π transition and its $I_{sFS}(\varphi)$ relationship can be really approximated by Eq. (5) with $A = -0.22I_{CI}$ and $B = 0.61I_{CI}$ [see Fig. 2(b)].

Substitution of this findings into (6) gives the $I_S(\varphi)$ presented in Fig. 2(a) by solid and dashed lines, which, respectively, corresponds to stable and unstable parts of $I_S(\varphi)$ curves calculated in the lumped junctions model for $I_{CI} = 0.88\pi T_C / R_N$, $A = -0.22I_{CI}$, and $B = 0.61I_{CI}$. We find a good match between the shapes of the curves calculated within the framework of these two approaches. The solutions of Eq. (6) shown by the dashed curves on the $I_S(\varphi)$ dependence correspond to the local maxima of $E(\chi)$. The system leaves these unstable states located at $\varphi/2\pi \approx 0.2$ and ≈ 0.8 through the resistive states of junctions and continuous change of the phase χ. In the vicinity of $\varphi \approx 2\pi$, the lumped junction model predicts the existence of two stable branches for the $I_S(\varphi)$ dependence. The first one corresponds to the line, with a positive derivative in the vicinity of $\varphi = 2\pi$. This branch is stable in the whole range of φ variation with two break hysteretic points $\varphi/2\pi \approx 0.2$; 0.8. The second branch of $I_S(\varphi)$ has a negative derivative for $\varphi = 2\pi$. This solution has stable parts only in the small vicinity of $\varphi = 2\pi$, while for the other parameter range, it is unstable [see the long dashed line on Fig. 2(a) stretching through the whole graph].

The microscopic approach permits to reach both branches depending on the initial conditions of the iterative calculation
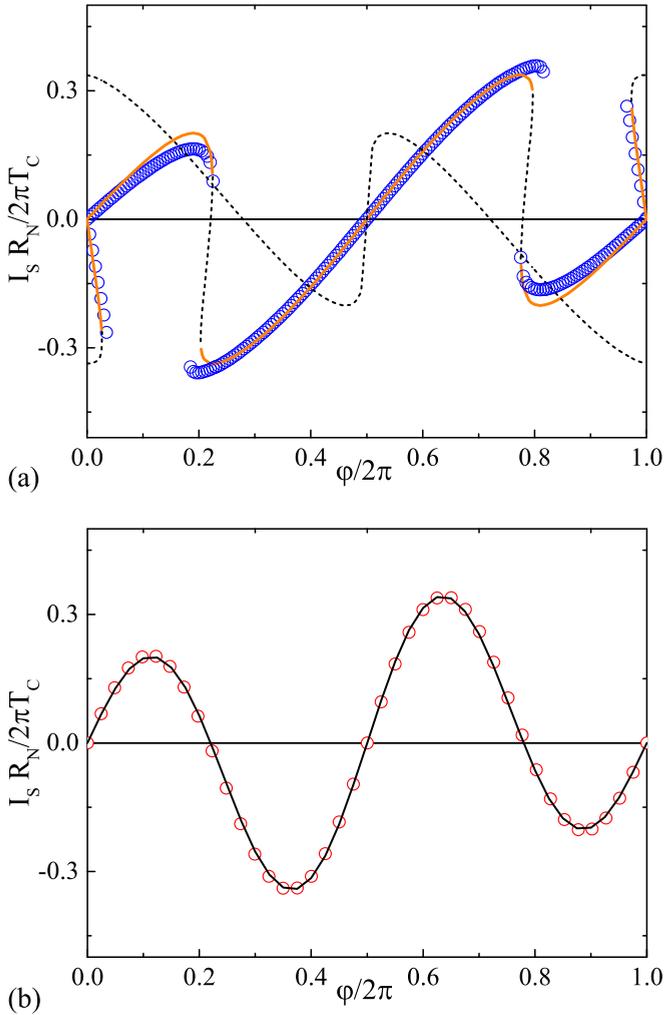
(a)

(b)

FIG. 2. The current-phase relation of the SIsFS (a) and sFS (b) junctions in the vicinity of 0-π transition. (a) shows comparison between the CPR following from solution of the Usadel equations (open circles) obtained for $d_F = 0.46\xi_S$, $d_s = 5\xi_S$, $H = 10\pi T_C$, $T = 0.2T_C$, and the CPR calculated in lumped junctions model for $A = -0.22I_{CI}$ and $B = 0.61I_{CI}$ (the solid and the dashed lines are stable and unstable parts of solution, respectively). The open circles in (b) give CPR of sFS junction calculated from the Usadel equations for the same set of the parameters and the fit is shown with the solid line for $A = -0.22I_{CI}$ and $B = 0.61I_{CI}$.

process. The realization of these two stable branches is shown in Fig. 2(a). The presence of stable intersecting branches in the $I_S(\varphi)$ dependence in the vicinity of $\varphi = 2\pi$ is a point for discussion. On the one hand, it leads to the potential instabilities caused by hopping between the stable states under the influence of the external noise environment, while on the other, the presence of such states is a precondition to the different applications in logic or memory devices. In any case, it is important to study and classify the variety of such multivalued states in junctions. To that end, we shall concentrate, hereafter, only on the analysis in the frame of lumped junctions model. As follows from Fig. 2, it may provide all stable and unstable branches of $I_S(\varphi)$ dependence, which fits reasonably well the exact result obtained from microscopic

theory. The latter requires much longer calculation time; especially, for the thick middle s layer and low temperatures due to slow convergence in the self-consistent iteration cycle. In addition, the result of the iterative process used to solve the microscopic problem is sensitive to the initial parameters, i.e., the initial phase of the intermediate s electrode. Finally, without loss of generality we will put below $I_{CI} = 1$ and consider A and B as independent parameters since near the 0-π transition the ratio of these factors is not fixed.

III. ANALYTICAL DESCRIPTION OF CPR

Equations (6)–(8) describing the lumped junction model can be solved analytically for some special cases. In the vicinity of T_C or in the limit of small thickness d_S, the amplitude B of the second harmonic is negligibly small compared to A, except in a very narrow parameter range for $A = 0$. As a result, we arrive at a serial connection of two junctions with sinusoidal CPR. In this case, the net $I_S(\varphi)$ relation is given by the well-known expression

$$I_S(\varphi) = \pm \frac{A \sin(\varphi)}{\sqrt{1 + A^2 + 2A \cos(\varphi)}}. \qquad (9)$$

The shape of this dependence becomes less sinusoidal, as the magnitude of A becomes close to unity; and for $A = 1$ the CPR given by Eq. (9) transforms into the piecewise function

$$I_S(\varphi) = \pm \sin(\varphi/2)sign(\cos(\varphi/2)). \qquad (10)$$

The minus sign in Eqs. (9) and (10) corresponds to unstable states. In these states, the phase of the order parameter of the core s layer differs by π on the order parameter phase in the superconducting electrodes. As a result, at least one of the contacts, connected in series, would be in an unstable state.

At low temperatures and at large d_S, there is an interval of parameters in the vicinity of 0 to π transition in which the contribution to the $I_S(\varphi)$ dependence from the first harmonic of the sFS junction is small compared to that from the second one. Taking $A \ll B$ in Eq. (6) and neglecting terms proportional to A, we can reduce (6) to a fourth-order equation with respect to $x = I_S(\varphi) = \sin(\chi)$:

$$4B^2x^4 + 4zx^3 + (1 - 4B^2)x^2 - 2zx + z^2 = 0, \qquad (11)$$

where $z = B \sin(2\varphi)$ and phase χ is in the interval $-\pi/2 < \chi < \pi/2$ if $u = zx(z - 2zx - x) > 0$ and is in the range $\pi/2 < \chi < 3\pi/2$ if $u < 0$. Below, we will compare the analytical expressions followed from (11) with the results of the numerical solution of Eqs. (6)–(8). They provide the phase χ as a function of φ presented in Fig. 3 for different values of B. The solid and dashed lines in Fig. 3 denote stable and unstable solutions, respectively.

In the limit $B \ll 1$, the weak place is located at the sFS part of SIsFS structure and for $\chi(\varphi)$ one can get

$$\chi \approx \frac{B \sin(2\varphi)}{1 + 2B \cos(2\varphi)}, \qquad (12)$$

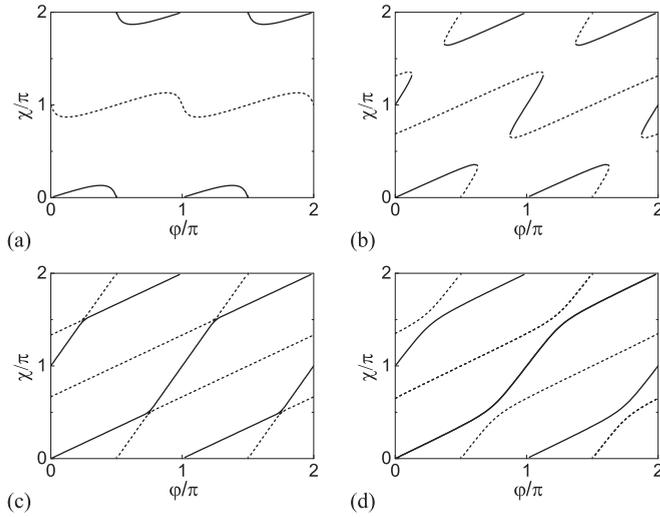$$\chi \approx \pi - \frac{B \sin(2\varphi)}{1 - 2B \cos(2\varphi)}. \qquad (13)$$

FIG. 3. The evolution of the phase χ of middle s-electrode order parameter as a function of total phase φ for the SIsFS junction calculated in the lumped junctions model for $A = 0$ and several values of the second harmonic amplitude $B = 0.4; 0.9; 1.0; 1.1$ [(a)–(d), respectively]. The shape of $\chi(\varphi)$ transforms from nonhysteretic ($B = 0.4$) to hysteretic ($B = 0.9$) dependence, which occurs before the merging point ($B = 1.0$). (c) gives $\chi(\varphi)$ at the merging point $B = 1.0$ and (d) shows a tunnel-like dependence $\chi(\varphi)$ above the merging point for $B = 1.1$.

The solution (12) is stable and corresponds to the solid curves located near $\chi = 2\pi n$, as shown in Fig. 3(a), calculated numerically from (11) for $B = 0.4$. The expression (13) gives the unstable solution shown by the dashed curve in Fig. 3(a). For $\chi \approx \pi$, the SIs tunnel junction in SIsFS device is in an energetically unfavorable π state, which is unstable.

Upon a further increase of the amplitude B [see Fig. 3(b)], the solution of Eq. (11) becomes hysteretic in the vicinity of $\varphi = 0 + \pi n$. For $\varphi = 0 + \pi n$, the coefficient $z = 0$, and Eq. (11) reduces to

$$\left(4B^2x^2 + 1 - 4B^2\right)x^2 = 0 \qquad (14)$$

and has three solutions

$$x_1 = 0, \quad x_{2,3} = \pm\sqrt{1 - 1/4B^2}. \qquad (15)$$

For $B \leqslant 0.5$, only x_1 is real and $I_S(\varphi)$ is a single-valued function of φ. In the interval $B > 0.5$, the $I_S(\varphi)$ dependence becomes a multivalued function of φ with three branches in the neighborhood of $\varphi = \pi + 2\pi n$. As will be demonstrated below, the appearance of an extra stable branch at $\chi \approx \pi$ can be explained due to the nucleation of local minimum at $\chi = \pi$ in the $E(\varphi)$ dependence, which corresponds to an energetically unfavorable stable state of the SIsFS structure. In this state, the SIs part of the structure is in the π state.

With the increase of B, the local minimum becomes deeper and at $B = 1$ the stable branches in $I_S(\varphi)$ merge together [see Fig. 3(c)]. At $B = 1$, the critical currents of SIs and sFS parts are equal to each other and Eq. (11) can be simplified to

$$(x + z)(4x^3 - 3x + z) = 0. \qquad (16)$$

Taking into account the restrictions on the intervals χ in Eq. (11), we can write the solutions of (16) in the form

$$\chi = \pi + 2\varphi, \qquad (17)$$

$$\chi = 2/3\varphi + 2/3\pi n, \qquad (18)$$

where $n = 0, 1$, and 2.

The equalities (17) and (18) provide a set of four intersecting linear relationships between phases χ and φ. The intersection points of these lines, as shown in Fig. 3(c), divide each of them into stable and unstable regions. Deviation of B from unity in the direction of smaller values leads to a separation of this linear solutions, as shown in Fig. 3(b). Contrary to this, with the increase of B, the weak place is shifted towards the SIs tunnel junction resulting in growth of χ with φ [see Fig. 3(d)]. The larger the value of B, the smaller is the deviation from the linear relation $\chi = \varphi + \pi n$ between χ and φ. It is important to note that the SIs tunnel junction can be both in a 0 state ($n = 0$) and π state ($n = 1$) depending on the condition in which the sFS contact is.

IV. NUMERICAL DESCRIPTION OF CPR

For the arbitrary values of amplitudes A and B, we solve Eqs. (6)–(8) numerically. We study the possible transformations of CPR shapes in the area $|A| \leqslant 1.5$, $|B| \leqslant 1.5$, which encloses the values of A and B at which the transition occurs between the 0 and π states in the SIsFS junction. A finite amplitude A results in the increase of the number of possible shapes of CPR in comparison with the discussion made above.

Below, we give a classification of the physical states implemented in the SIsFS structures based on two criteria. The first one includes the classification of the ground states. Those are the states that meet the requirements of the minimum of the functional $E(\varphi)$ and of the stability [Eq. (8)]. In addition, we do not take into account the minima, which have energy larger than the energy of any other branch at the same φ. The second criterion specifies information about the shape of the $I_S(\varphi)$ curves. It gives the number, k, of stable branches of $I_S(\varphi)$ unconnected with one another, as well as the number, m, of possible jumps caused by the transition between these branches arising during φ, swiping in the interval $0 \leqslant \varphi \leqslant 2\pi$.

There are four possible types of ground states of SIsFS structure. Their examples, as well as the corresponding $I_S(\varphi)$ relationships are shown in Fig. 4. The implementation of 0 or π states depends mainly on the relationship between the amplitudes $2|B|$ and $|A|$ (see Fig. 5). For $|A| > 2|B|$, the SIsFS structure has a single ground state at $\varphi = 0$ at positive A, and at $\varphi = \pi$ at negative A. Figures 4(a) and 4(b) reveal the $E(\varphi)$ and $I_S(\varphi)$ calculated for $B = 0$ and $A = \pm 1.4$, respectively. At $A = 1.4$, the minimum of $E(\varphi)$ is achieved at $\varphi = 0 + 2\pi n$, while for $A = -1.4$ it is shifted towards $\varphi = \pi + 2\pi n$. We have identified these ground states as 0 and π, respectively. These types of CPRs can be also observed in the regular SFS and S-F/N-S junctions [2]. However, in the SIsFS junctions, the shapes of $I_S(\varphi)$ significantly deviate from the sinusoidal one even in the absence of the second harmonics ($B = 0$).

Figures 4(c) and 4(d) show the $E(\varphi)$ and $I_S(\varphi)$ calculated for $B = \pm 0.4$ and $A = 0.1$, respectively. For positive B, the
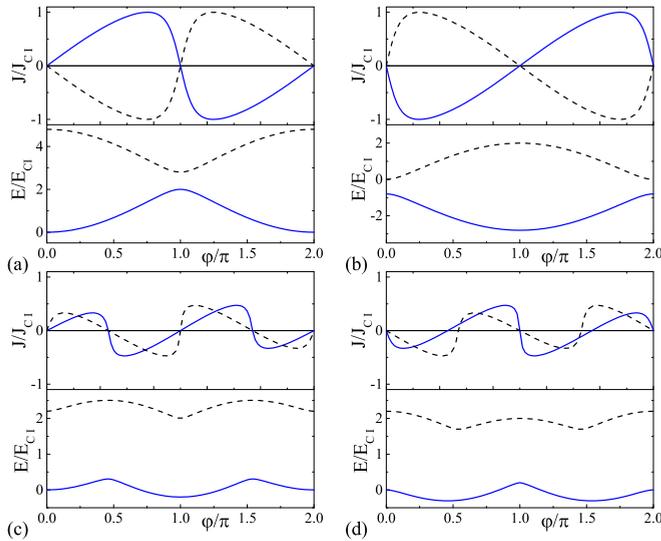
FIG. 4. The current-phase (top) and the energy-phase (bottom) relations of SIsFS junction calculated in the lumped junctions model for combinations of amplitudes A and B provided trivial single-valued shape of CPR: (a) 0-ground state at $A = 1.4$, $B = 0$, (b) π state at $A = -1.4$, $B = 0$, (c) 0-π-ground state at $A = 0.1$, $B = 0.4$, (d) φ-ground state at $A = 0.1$, $B = -0.4$. It is seen that, serial connection of SIs and sFS junctions provides significant deviations of CPR from sinusoidal shape even in the absence of the second harmonic.

$E(\varphi)$ curve [see Fig. 4(c)] has two minima at $\varphi = 0$ and π. We classify this situation as 0-π ground state [10,11]. The diagram in Fig. 5 shows that a 0-π ground state exists if $|A| < 2|B|$ and $|A| < 1$. The case $|A| > 1$ is less trivial and will be discussed below.
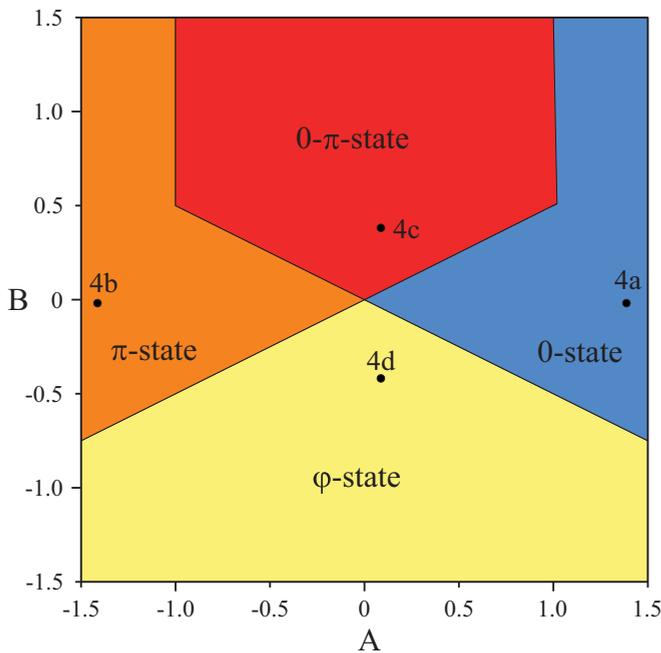

FIG. 5. Ground-state distribution in the SIsFS structures on (A, B) phase plane.

For $|A| < 2|B|$ and $B < 0$, the $E(\varphi)$ curve (see Fig. 5) reaches a global minimum at some arbitrary phase $\varphi = \pm\varphi_g$, which does not coincide with both $\varphi = 0$ and $\varphi = \pi$. Figure 4(d) demonstrates an example of this situation realized for $A = 0.1$ and $B = -0.4$. For small $|B| \ll 1$, the properties of an SIsFS junction are similar to that of the so-called φ junction [12], such that the magnitude of φ_g can be any value in the range $[0,\pi]$. With increase of $|B|$, the interval available for φ_g diminishes and for $|B| \gg 1$ it asymptotically converges to $\pm\pi/2$. It is necessary to note that the condition $B < 0$ can be realized in junctions with a complex internal structure of their weak link region [12–17].

Contrary to the result presented in Fig. 2, all the $I_S(\varphi)$ dependencies shown in Fig. 4 are single-valued functions of φ. These types of current-phase relations exist only in the limited area in the (A, B) phase plane. It means that the phase diagram in Fig. 5 is rather crude. It requires a further clarification of the boundaries separating the areas of single-valued and multivalued current phase relations.

For further determination of possible CPR, we need to introduce additional parameters. They are indices k and m. As defined above, the index k counts the number of stable branches of $I_S(\varphi)$ including ground states and unconnected with another branch geometrically, so that switching of the system from one branch to another is possible only through a phase slip. The index m gives the number of possible jumps caused by the transition between these branches arising during φ increase in the interval $0 \leqslant \varphi \leqslant 2\pi$. We determine it as the number of phase slips during a continuous increase of phase φ, starting from the position at the ground state. The counting ends at a value of φ that is different from the initial one by 2π even if the systems stays on the other branch with further increase of φ. In this way, the number m_i is found for each ground state. The resulting index $m = \sum m_i$ is a sum over existing ground states.

The classification is summarized in Fig. 6, which presents the information on the number of hysteretic regions in the $I_S(\varphi)$ dependence, and also on the mutual positions of the ground states and phase jumps. The filled black circles in the plane are the points at which the CPR presented in Figs. 4 and 7–10 has been calculated in the frame of the lumped junctions model. The number of the corresponding figure is written near the circles.

Figures 7–10 demonstrate the main classes of the current-phase relations. In the diagram presented in Fig. 6 they are marked by different colors. Each panel in Figs. 7–10 gives $I_S(\varphi)$ and $E_S(\varphi)$ dependencies calculated numerically from Eq. (6). As in Fig. 3, the dashed black lines show unstable states. Different colors of solid lines correspond to the different branches of stable solutions. From Fig. 6, it is seen that for positive B, $I_S(\varphi)$ transforms into a multivalued function for $B \gtrsim 0.5$ and $|A| \lesssim 0.75$.

Typical $I_S(\varphi)$ and $E_S(\varphi)$ curves for the area 7 in Fig. 6(a) are shown in Fig. 7. They have been calculated for $A = 0.1$ and $B = 0.8$. The current-phase relation consists of two stable branches leading to $k = 2$. In the domain $0 \leqslant \varphi \leqslant 2\pi$, a phase sweep from 0 to 2π must lead to two hops between stable branches for each of the two available ground states resulting in $m = 4$. It is necessary to note that in this area of parameters A and B there are some additional stable branches at higher
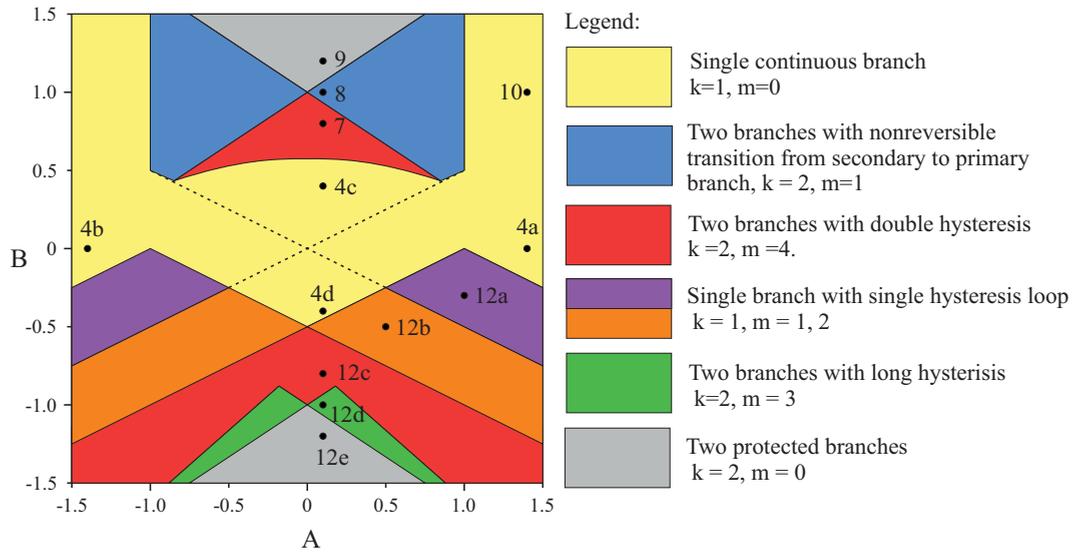
FIG. 6. Distribution of indices of the SIsFS junction CPR in the (A, B) phase plane. The legend reveals the correspondence between the colors and the indices: k is the number of stable branches of $I_S(\varphi)$ including ground states, which are unconnected with each other geometrically; m gives the number of possible jumps caused by the transition between these branches arising during φ increase in the interval $0 \leqslant \varphi \leqslant 2\pi$. The dashed lines define the boundary between different types of ground states. The filled black circles in the plane are the points at which the CPR presented in Figs. 4 and 7–10 has been calculated in the frame of the lumped junctions model. The number of the corresponding figure is written near the circles. The shapes of CPR for negative B are presented in Appendix in Fig. 12.

energies (orange lines on Fig. 7, which do not correspond to the ground state). Due to large energy difference between these states it is impossible to switch between them by an adiabatic change of the phase φ.

Figure 8 gives an example of $I_S(\varphi)$ and $E_S(\varphi)$ curves typical for area 8 in A-B plane in Fig. 6. They have been calculated for $A = 0.1$ and $B = 1$. At $B = 1$, the shapes of $I_S(\varphi)$ and $E_S(\varphi)$ dependencies exhibit a transition to a state with $k = 2$ and $m = 1$. With increase of B, the stable branches corresponding to the

minimum energy (marked by blue in Fig. 7) tend to connect to the stable branches corresponding to the maximum energy (marked by orange in Fig. 7 in a vicinity of $\varphi = \pi$). For the particular case of $A = 0.1$ shown in Fig. 8, the connection has completed at $B = 1$ resulting in formation of the continuous $I_S(\varphi)$ and $E_S(\varphi)$ dependencies without any hysteresis. For

FIG. 8. The current-phase relation (top) and energy-phase relation (bottom) for the SIsFS structure in the state with primary branch $k = 2$ and $m = 1$ calculated for $A = 0.1$ and $B = 1.0$. The solid lines correspond to stable states. The blue line corresponds to a ground state at $\varphi = 0$. It is the primary branch, which is stable in the whole range of variation $0 \leqslant \varphi \leqslant 2\pi$. The red line is the secondary branch, stable parts of which exist only in some interval of φ in the vicinity of $\varphi = \pi$. The orange line located nearby $\varphi = 0$ shows energetically higher states with the π shift across the SIs tunnel junction. The dashed lines show unstable states.
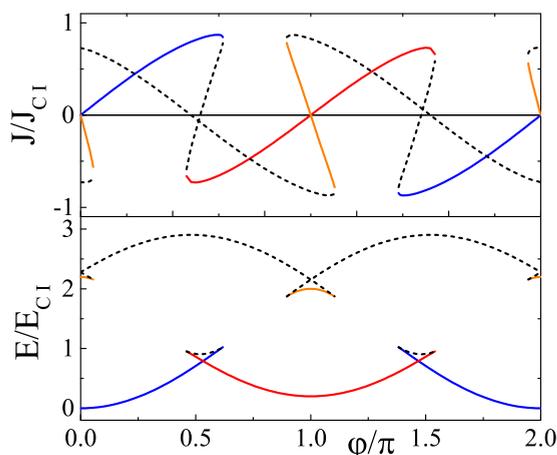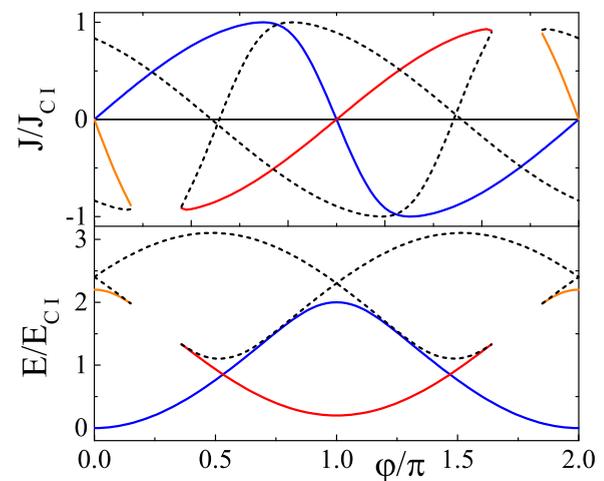

FIG. 7. The current-phase relation (top) and the energy-phase relation (bottom) for the SIsFS structure in hysteretic state $k = 2$ and $m = 4$ calculated for $A = 0.1$ and $B = 0.8$. The solid lines correspond to stable states. The blue line is a branch including a ground state $\varphi = 0$, the red line corresponds to a ground state $\varphi = \pi$, and two orange lines show energetically higher states with π shift across the SIs tunnel junction. The dashed lines show unstable states.
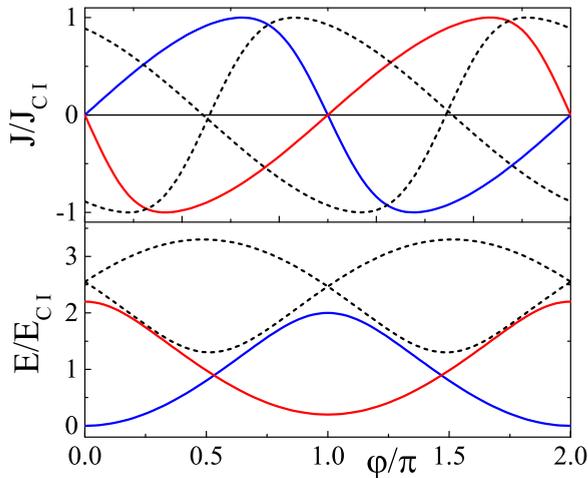
FIG. 9. The current-phase relation (top) and the energy-phase relation (bottom) for the SIsFS structure in the state with two independent protected branches $k = 2$ and $m = 0$ calculated in the lumped junctions model for $A = 0.1$ and $B = 1.2$. Solid lines show the stable states. Blue and red lines correspond to the branches having ground state at $\varphi = 0$ and π, respectively. Both branches exist for all φ in the range $0 \leqslant \varphi \leqslant 2\pi$. By an adiabatic change of the phase φ it is impossible to switch between these two branches. The dashed lines show unstable states.
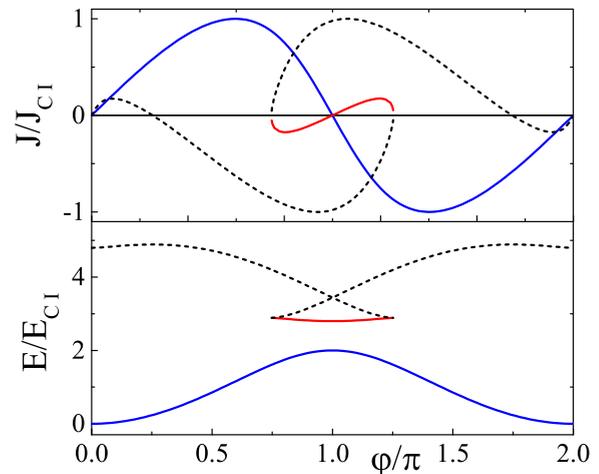

FIG. 10. The blue lines show a current-phase relation (top) and the energy-phase relation (bottom) for the SIsFS structure with multivalued CPR shape ($k = 1$ and $m = 0$) having a single ground state at $\varphi = 0$. The red lines show the analogous curves for energetically unfavorable states. It is seen that a metastable state at $\varphi = \pi$ is also possible. The dashed lines show unstable states. The calculation is done in the lumped junctions model for $A = 1.4$ and $B = 1.0$.

finite A, the minima of $E(\varphi)$ at $\varphi = 0$ and $\varphi = \pi$ have different depth ($E(0) < E(\pi)$) and corresponding merging points split at $B_{1,2} = 1 \pm 2/3\,A$. In the interval $B_1 \leqslant B \leqslant B_2$ and at $|A| < 1$, the branch of $E(\varphi)$ passing through a deeper minimum is already continuous at every φ, while the second branch of $E(\varphi)$ exists only in some intervals of φ (see Fig. 8). An escape of phase φ from these intervals leads to the jump of E on a more stable $E(\varphi)$ branch. After that, the SIsFS junction can not be adiabatically switched back into the previous state.

The next transition to the state with $k = 2$ and $m = 0$ occurs for $|A| < 1$ and the amplitude B exceeds B_2 (Fig. 9). In this area of amplitudes, the weak place is located at the SIs junction, while the SIsFS structure can stay either in 0 or in π state. One of the two energetically favored states corresponds to the global minimum of the energy at $\varphi = 0$, while the second corresponds to a local minimum at $\varphi = \pi$. The magnitudes of $E(\varphi)$ at $\varphi = 0$ and $\varphi = \pi$ are slightly different. These states are protected from each other in the sense that a transition from one of them to another is not possible with a continuous adiabatic phase change of φ. To switch SIsFS junction between the 0 and π states, one should increase a bias current across the junction to a value larger than the critical current of sFS part of the structure.

Finally, the region with $|A| > 1$ corresponds to the dependence shown in Fig. 10. The CPR in this state also has two branches with minima on the $E(\varphi)$ dependence. However, the split between branches is too large, and the local minimum of the upper branch is energetically higher than the maximum of the lower branch. Thus the upper local minimum can not be declared as a possible ground state, and we do not count this branch in indices k and m. In this way, we call the states at $|A| > 1$ as 0 and π states on the phase diagram in Fig. 5

and consider it as the state with the single branch $k = 1$ in Fig. 6(a).

The current-phase relations with a negative sign of the second harmonic amplitude B are less common and require the realization of a complex F region consisting from a number of layers [12–16]. Therefore we shift the discussion of the classification of the states shown at the bottom half of the diagram in Fig. 6 to Appendix.

The above classification of CPR may help to interpret the experimental data in the SIsFS structures near 0 to π transitions. In standard SFS junctions, 0-π transitions manifest themselves as dips in the $I_C(d_F)$ or $I_C(T)$ dependencies. Experimental results for SIsFS junctions demonstrate similar behavior in the regime of small thickness d_s. However, such dips disappear for large d_s (see Ref. [6]).

To explain this effect, we consider the dependence of the critical current I_C on the first harmonic amplitude A for several fixed values of the second harmonic B as shown in Fig. 11. In the absence of the second harmonic (the solid line), the pronounced dip of I_C is visible, indicating 0 to π transition. In the parameter range within the dip, the weak link is shifted from the tunnel barrier I to the ferromagnetic layer F. Far from the 0-π transition, the magnitude of I_C is independent on A and equals to the critical current of the SIs tunnel junction, where the weak link is located.

With the increase of B, the CPR deforms and additional branches start to appear. As a consequence, the dips at $I_C(A)$ curves gradually decrease (see the red dashed and the blue dash-dot lines on Fig. 6). Finally, at $B > 1$, the dip vanishes and the weak link is always located at the tunnel barrier. As a result, I_C remains constant across the 0-π transition (the orange dash-dot-dot line).

As follows from the above discussion, the standard approach for detection of 0-π transitions, based on measurements
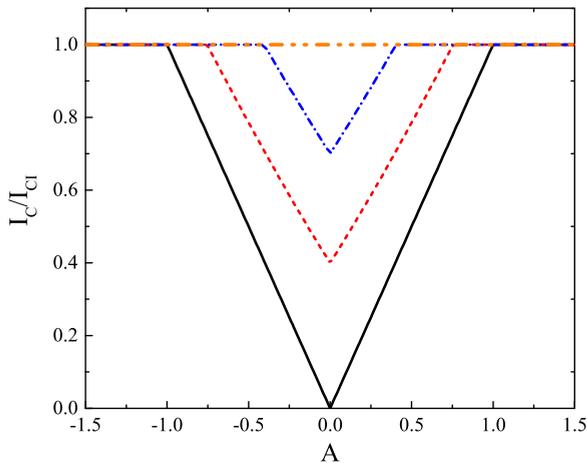
FIG. 11. The dependence of the critical current I_C on the amplitude of the first CPR harmonic A during the 0-π transition in SIsFS junction. The 0-π transition is defined as a change of A sign under the condition of fixed second harmonic amplitude B. Solid black, dashed red, dash-dot blue, and dash-dot-dot orange lines correspond to $B = 0; 0.4; 0.7$ and $B \geqslant 1$, respectively.

of $I_C R_N(d_F)$ dependencies, breaks down in SIsFS junctions at low temperatures and large s-layer thickness $\gtrsim 3\xi_S$. Detection of such transitions requires phase-sensitive experiments [7].

V. CONCLUSION

As follows from our analysis, the CPR in the SIsFS structures is qualitatively different from that in regular SFS junctions. We have demonstrated that the classification of the various CPR types requires the use of two indices. One of them, k, indicates the number of the existing ground states, while the other, m, defines the number of current leaps occurring during variation of the phase difference φ in each of these ground states from 0 to 2π. We have also shown that the values of these indices depend on the ratio between the amplitudes of the first A and second B harmonics in CPR of the sFS part of the SIsFS junction. We have identified the areas in the A-B plane corresponding to all possible combinations of pairs of these indices, as well as the typical shapes of the CPR for each of these areas. We have shown that some of the found states are protected. An example is given in Fig. 9, which depicts two CPR in the protected state with indices $k = 2$ and $m = 0$. In this case, the SIsFS structure can stay either in 0- or in π-ground state, with only slight difference between the magnitudes of $E(\varphi)$ at $\varphi = 0$ and $\varphi = \pi$. Furthermore, a transition from one ground state to another is not possible by a continuous adiabatic variation of the phase φ. Our preliminary analysis done in the frame of the RSJ model confirms that this property is conserved even in a dynamic regime, despite the existence of a voltage drop across the SIsFS junction and the fact that both χ and φ are time dependent. To switch the SIsFS junction between the 0 and π states, one should increase a bias current across the junction to a value larger than the critical current of the sFS part of the structure. More detailed consideration of switching between protected CPR branches will be done elsewhere.

Note that there is some similarity between the considered properties and the effects found in the topological systems based on multiterminal Josephson junctions [18–20]. In the latter case, different topological states correspond to different distributions of phase differences between the terminals. In SIsFS junctions, an intermediate electrode can be considered as an additional terminal embedded into the SIFS weak link. The resulting states of SIsFS contacts become separated and any transition between them should be accompanied by a flux flow across the SIs or the sFS parts of the structure.

It is necessary to mention that the results of our investigation may be also important from the application point of view. Hybrid structures combining ferromagnetic and superconducting layers became subjects of intensive study in recent years [2,21–23]. Superconducting correlations induced into a ferromagnetic region by the proximity effect can be controlled by an effective exchange field, leading to a number of practically important phenomena, such as spin-valve effects [24–34], which look rather promising for superconducting electronics [35,36]. In addition, there is a class of memory devices that operate without performing the magnetization reversal of the ferromagnetic layer [37–40]. The SIsFS junctions are also considered as possible candidates for memory elements. [6,41–43]. They have a noticeable advantage compared to standard pseudo-spin-valve devices [33]. Their $I_C R_N$ product is of the same order as that of the Josephson elements used in RSFQ logic circuits. In addition, SIsFS junctions can be used as superconducting transistors [44,45], where the magnitude and the phase of the order parameter in the middle s-layer are controlled by spin injection from the F film. The effective magnetic layer F in these structures can be realized as a composite structure including several magnetic layers separated by normal or superconductive spacers [46–49]. It is important that the performed investigations of the current phase relation in SIsFS junctions provide a solid base for understanding the modes of operation of these transistors and memory elements.

APPENDIX: CLASSIFICATION OF THE STATES AT NEGATIVE *B*

Current phase relation with negative sign of the second harmonic amplitude B in the sFS junction can be realized only in the case of a more complicated weak link region. It requires additional inhomogeneity inside the F layer. For instance, the existence of normal metal areas or steplike geometry of the layer [12–17].
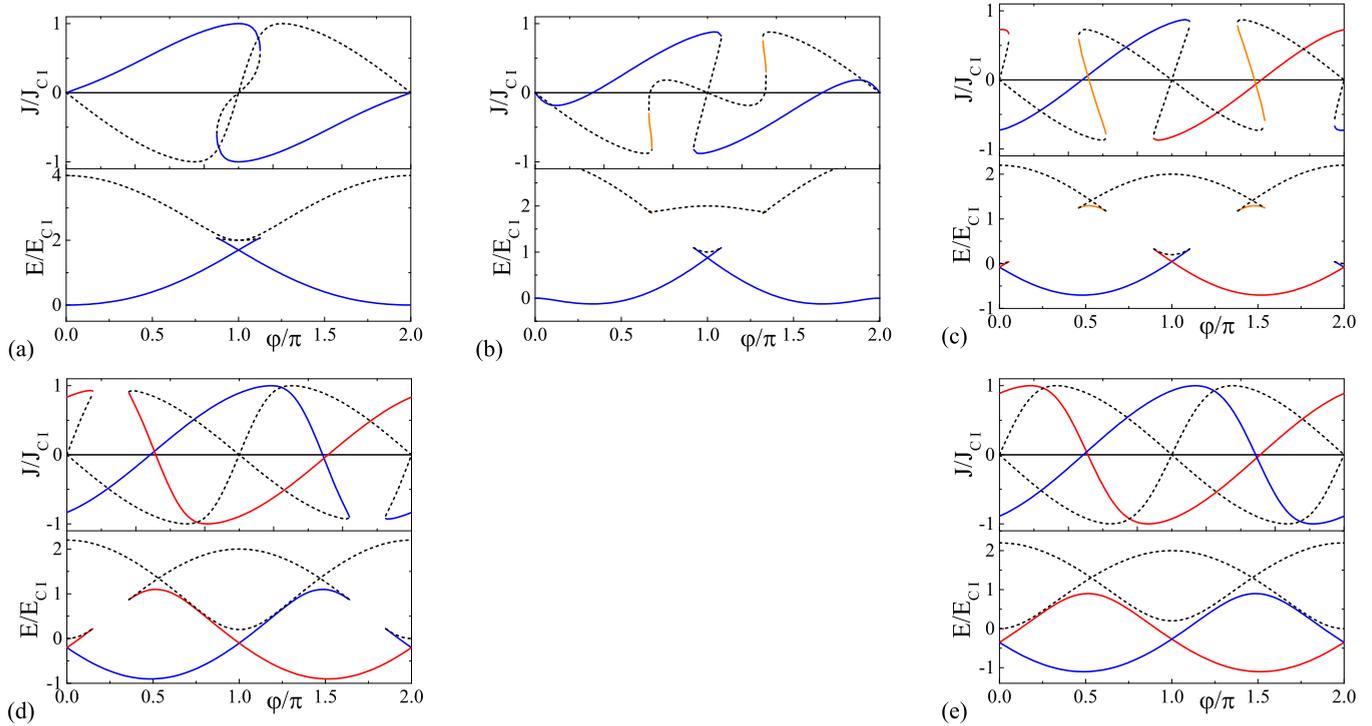
FIG. 12. The current-phase and the energy-phase relations for different states of the SIsFS junction with negative amplitudes of the second harmonic $B < 0$: (a) 0-ground state with single hysteresis $k = 1, m = 1$ at $A = 1.0$, $B = -0.3$ and (b) double-well branch with single hysteresis $k = 1, m = 2$ at $A = 0.5$, $B = -0.5$; (c) hysteretic φ state with double hysteresis $k = 2, m = 4$ at $A = 0.1$, $B = -0.8$; (d) φ with long hysteresis-state $k = 2, m = 3$ at $A = 0.1$, $B = -1.0$; (e) protected φ state $k = 2, m = 0$ at $A = 0.1$, $B = -1.2$. Solid lines and dashed lines show stable and unstable states, respectively.

Generally, the sign change of B leads to a symmetrical transformation of CPR:

$$I_S(\varphi, A, B) = -I_S(\varphi, A, -B), \tag{A1}$$

$$E(\varphi, A, B) = -E(\varphi, A, -B). \tag{A2}$$

The sign change of the energy in Eq. (13) significantly influences the condition of stability (8). Every stable solution for positive B becomes unstable after transformation to negative B and vice versa. This general property determines the significant difference between the distributions of states with $B > 0$ and $B < 0$ on the phase plane in Fig. 6.

Our analysis has shown that, for negative values of amplitude B, some new types of the states may exist (see bottom part of Fig. 6). Figures 12(a)–12(e) demonstrate the main classes of the current-phase relations existing for $B < 0$. Each panel in Figs. 12(a)–12(e) gives $I_S(\varphi)$ and $E(\varphi)$ dependencies calculated numerically from Eq. (6). The dashed black lines show unstable states. Different colors of the solid lines correspond to different branches of stable solutions. The filled black circles in the plane in Fig. 6 are the points at which the CPR presented in Figs. 12(a)–12(e) have been calculated in the frame of lumped junctions model. The number of the corresponding pannel in Figs. 12(a)–12(e) is written near the circles.

Typical $I_S(\varphi)$ and $E(\varphi)$ curves for the area restricted by the three lines $B = 0.5 - 0.5|A|$, $B = -0.5 + 0.5|A|$, and $B = -0.5|A|$ in the A-B plane are shown in Fig. 12(a). They have been calculated for $A = 1.0$ and $B = -0.3$. It is seen that

$I_S(\varphi)$ is a continuous function of φ practically for all φ except for the area in the vicinity of $\varphi = \pi$, where the current leap takes place. Figure 12(a) shows that there is one ground state in $E(\varphi)$ at $\varphi = 0$ and one hysteresis in $I_S(\varphi)$ resulting in $k = 1$ and $m = 1$.

The considered A-B area provides the first example of the difference in the SIsFS junction characteristics between the cases of positive and negative B. For $A = 1.0$ and $B = 0.3$, there are two hysteresis loops in $I_S(\varphi)$ relation, while for $A = 1.0$, $B = -0.3$, there is a single hysteresis loop in CPR. The second hysteresis in $I_S(\varphi)$ forms afterwards, during further $|B|$ increase. However, the first effect that appears with $|B|$ increase is transformation of the SIsFS structure into a φ junction having two ground states in the $E(\varphi)$ dependence, as it is shown in Figs. 12(b)–12(e).

It is seen that the energy $E(\varphi)$ has two minima at some arbitrary phases $\varphi = \varphi_g$ and $2\pi - \varphi_g$, so that $E(\varphi_g) = E(2\pi - \varphi_g)$. This phase φ_g does not coincide with both $\varphi = 0$ and π and rapidly saturates at $\varphi_g = \pi/2$ with increasing $|B|$.

The initial stage of φ-state formation is shown in Fig. 12(b). It is seen that $I_S(\varphi)$ also has a single branch with single hysteresis ($k = 1$), but there are two ground states in $E(\varphi)$ curve, summation over which gives index $m = 2$. Figure 12(b) demonstrates that the dependencies are typical for SIsFS contacts if the sFS junction parameters located inside the area restricted by the three lines in A-B plane. They are $B = -0.5 - 0.5|A|$, $B = -0.5 + 0.5|A|$, and $B = -0.5|A|$.

After crossing the line $B = -0.5 - 0.5|A|$ with further $|B|$ increase, the second hysteresis is nucleating in the

current-phase relation in a vicinity of $\varphi = 0$. Typical $I_S(\varphi)$ and $E(\varphi)$ curves for this range of parameters is demonstrated in Fig. 12(c). The calculations have been done for $A = 0.1$ and $B = -0.8$. There is a direct correspondence between the stable part of the $I_S(\varphi)$ curve and the corresponding ground state in $E(\varphi)$. This CPR is characterized by $k = 2$ and $m = 4$. It is similar to that shown above in Fig. 7.

With further $|B|$ growth, the φ range of the stable ground solutions increases [blue and red lines on Fig. 12(c)]. These branches tend to merge with high energy curves [orange lines on Fig. 12(c)]. However, this merging does not occur simultaneously for left and right ends of the stable $E(\varphi)$ dependencies. This leads to the formation of a narrow range of parameters, where high-energy branches are connected to the ground branches only from the one end of the stable curve, as it is shown in Fig. 12(d). The calculations have been done for $A = 0.1$ and $B = -1.0$. The corresponding current-phase relation has a long hysteresis, which provides different indices m_i for different ground states. While we count the number of current jumps during a continuous increase of phase φ for the left ground state in Fig. 12(d) going along the blue line, the result is the same with the later case, $m_1 = 2$. However, the index for the ground state at $\varphi = \pi/2$ on the red line is equal to unity $m_2 = 1$. The system jumps on the blue line near the phase $\varphi \approx 0.2 + 2\pi$ and stays on it until $\varphi = \pi/2 + 2\pi$. Thus the total hysteresis index $m = 3$ is odd for this state, while $k = 2$ is still the same. An additional consequence of this property is the dependence of the existing state upon the direction of the variation of the phase φ. If we increase φ, the system principally stays on the blue line. However, the state on the red line becomes more probable during the decrease in phase φ.

Finally, for $B < -1 - 2/3|A|$, the system goes in the φ state with protected $I_S(\varphi)$ branches, which are characterized by $k = 2$ and $m = 0$ [see Fig. 12(e)]. There are two independent 2π periodical $I_S(\varphi)$ curves corresponding to the ground states in the vicinity $\pi/2$ and $-\pi/2$, respectively. The calculations have been done for $A = 0.1$ and $B = -1.2$.

[1] K. K. Likharev, Rev. Mod. Phys. **51**, 101 (1979).

[2] A. A. Golubov, M. Yu. Kupriyanov, and E. Il'ichev, Rev. Mod. Phys. **76**, 411 (2004).

[3] K. K. Likharev and L. A. Yakobson, Zh. Tekhn. Fiz. **45**, 1503 (1975) [Sov. Phys. Tech. Phys. **20**, 950 (1975)].

[4] M. Yu. Kupriyanov, K. K. Likharev, and L. A. Maslova, in *Proceedings of the 14th International Conference on Low Temperature Physics*, edited by M. Krusius and M. Vuorio, 14-20 August (Amsterdam Netherlands; Otaniemi Finland: North-Holland, The Netherlands, 1975), Vol. 4, p. 104.

[5] S. V. Bakurskiy, N. V. Klenov, I. I. Soloviev, M. Yu. Kupriyanov, and A. A. Golubov, Phys. Rev. B **88**, 144519 (2013).

[6] N. Ruppelt, H. Sickinger, R. Menditto, E. Goldobin, D. Koelle, R. Kleiner, O. Vavra, and H. Kohlstedt, Appl. Phys. Lett. **106**, 022602 (2015).

[7] S. M. Frolov, D. J. Van Harlingen, V. A. Oboznov, V. V. Bolginov, and V. V. Ryazanov, Phys. Rev. B **70**, 144505 (2004).

[8] K. D. Usadel, Phys. Rev. Lett. **25**, 507 (1970).

[9] M. Yu. Kuprianov and V. F. Lukichev, Zh. Eksp. Teor. Fiz. **94**, 139 (1988); [Sov. Phys. JETP **67**, 1163 (1988)].

[10] Z. Radovic, L. Dobrosavljevic-Grujic, and B. Vujicic, Phys. Rev. B **63**, 214512 (2001).

[11] Z. Radovic, N. Lazarides, and N. Flytzanis, Phys. Rev. B **68**, 014501 (2003).

[12] A. Buzdin and A. E. Koshelev, Phys. Rev. B **67**, 220504(R) (2003).

[13] N. G. Pugach, E. Goldobin, R. Kleiner, and D. Koelle, Phys. Rev. B **81**, 104513 (2010).

[14] E. Goldobin, D. Koelle, R. Kleiner, and R. G. Mints, Phys. Rev. Lett. **107**, 227001 (2011).

[15] S. V. Bakurskiy, N. V. Klenov, T. Yu. Karminskaya, M. Yu. Kupriyanov, and A. A. Golubov, Supercond. Sci. Technol. **26**, 015005 (2013).

[16] H. Sickinger, A. Lipman, M. Weides, R. G. Mints, H. Kohlstedt, D. Koelle, R. Kleiner, and E. Goldobin, Phys. Rev. Lett. **109**, 107002 (2012).

[17] R. Menditto, H. Sickinger, M. Weides, H. Kohlstedt, M. Zonda, T. Novotny, D. Koelle, R. Kleiner, and E. Goldobin, Phys. Rev. B **93**, 174506 (2016).

[18] E. Strambini, S. D'Ambrosio, F. Vischi, F. S. Bergeret, Y. V. Nazarov, and F. Giazotto, Nat. Nanotechnol. **11**, 1055 (2016).

[19] M. Amundsen, J. A. Ouassou, and J. Linder, Sci. Rep. **7**, 40578 (2017).

[20] F. Vischi, M. Carrega, E. Strambini, S. D'Ambrosio, F. S. Bergeret, Yu. V. Nazarov, and F. Giazotto, Phys. Rev. B **95**, 054504 (2017).

[21] M. G. Blamire, and J. W. A. Robinson, J. Phys.: Condens. Matter **26**, 453201 (2014).

[22] M. Eschrig, Rep. Prog. Phys. **78**, 104501 (2015).

[23] J. Linder, and J. W. A. Robinson, Nat. Phys. **11**, 307 (2015).

[24] L. R. Tagirov, Phys. Rev. Lett. **83**, 2058 (1999).

[25] A. I. Buzdin, A. V. Vedyayev, and N. V. Ryzhanova, Europhys. Lett. **48**, 686 (1999).

[26] M. A. El Qader, R. K. Singh, S. N. Galvi, L. Yu, J. M. Rowell, and N. Newman, Appl. Phys. Lett. **104**, 022602 (2014).

[27] Ya. V. Fominov, A. A. Golubov, and M. Yu. Kupriyanov, Pis'ma Zh. Eksp. Teor. Fiz. **77**, 609 (2003) [JETP Lett. **77**, 510 (2003)].

[28] Ya. V. Fominov, A. A. Golubov, T. Yu. Karminskaya, M. Yu. Kupriyanov, R. G. Deminov, and L. R. Tagirov, Pis'ma Zh. Eksp. Teor. Fiz. **91**, 329 (2010) [JETP Lett. **91**, 308 (2010)].

[29] S. V. Mironov and A. Buzdin, Phys. Rev. B **89**, 144505 (2014).

[30] F. S. Bergeret, A. F. Volkov, and K. B. Efetov, Rev. Mod. Phys. **77**, 1321 (2005).

[31] M. Houzet and A. I. Buzdin, Phys. Rev. B **76**, 060504(R) (2007).

[32] M. Alidoust and J. Linder, Phys. Rev. B **82**, 224504 (2010).

[33] B. Baek, W. H. Rippard, S. P. Benz, S. E. Russek, and P. D. Dresselhaus, Nat. Commun. **5**, 3888 (2014).

[34] I. I. Soloviev, N. V. Klenov, S. V. Bakurskiy, V. V. Bol'ginov, V. V. Ryazanov, M. Yu. Kupriyanov, and A. A. Golubov, Appl. Phys. Lett. **105**, 242601 (2014).

[35] J. W. Lu, E. Chen, M. Kabir, M. R. Stan, and S. A. Wolf, Int. Mater. Rev. **61**, 456 (2016).

[36] S. K. Tolpygo, Fiz. Nizk. Temp. **42**, 463 (2016) [Low Temp. Phys. **42**, 361 (2016)].

[37] E. Goldobin, H. Sickinger, M. Weides, N. Ruppelt, H. Kohlstedt, R. Kleiner, and D. Koelle, Appl. Phys. Lett. **102**, 242602 (2013).

[38] T. Golod, A. Iovan, and V. M. Krasnov, Nat. Commun. **6**, 8628 (2015).

[39] S. V. Bakurskiy, N. V. Klenov, I. I. Soloviev, M. Yu. Kupriyanov, and A. A. Golubov, Appl. Phys. Lett. **108**, 042602 (2016).

[40] A. Murphy, D. Averin, and A. Bezryadin, arXiv:1701.08715.

[41] T. I. Larkin, V. V. Bol'ginov, V. S. Stolyarov, V. V. Ryazanov, I. V. Vernik, S. K. Tolpygo, and O. A. Mukhanov, Appl. Phys. Lett. **100**, 222601 (2012).

[42] I. V. Vernik, V. V. Bol'ginov, S. V. Bakurskiy, A. A. Golubov, M. Yu. Kupriyanov, V. V. Ryazanov, and O. A. Mukhanov, IEEE Trans. Appl. Supercon. **23**, 1701208 (2013).

[43] S. V. Bakurskiy, N. V. Klenov, I. I. Soloviev, V. V. Bol'ginov, V. V. Ryazanov, I. I. Vernik, O. A. Mukhanov, M. Yu. Kupriyanov, and A. A. Golubov, Appl. Phys. Lett. **102**, 192603 (2013).

[44] I. P. Nevirkovets, O. Chernyashevskyy, G. V. Prokopenko, O. A. Mukhanov, and J. B. Ketterson, IEEE Trans. Appl. Supercon. **24**, 4 (2014).

[45] S. Shafranjuk, I. P. Nevirkovets, and O. A. Mukhanov, and J. B. Ketterson, Phys. Rev. Appl. **6**, 024018 (2016).

[46] S. V. Bakurskiy, M. Yu. Kupriyanov, A. A. Baranov, A. A. Golubov, N. V. Klenov, and I. I. Soloviev, JETP Lett. **102**, 586 (2015).

[47] M. Alidoust and K. Halterman, Phys. Rev. B **89**, 195111 (2014).

[48] K. Halterman, and M. Alidoust, Supercond. Sci. Technol. **29**, 055007 (2016).

[49] J. A. Ouassou and J. Linder, arXiv:1612.03177.